Pion-less effective field theory on low-energy deuteron electrodisintegration

Stefan Christlmeier[1] and Harald W. Grießhammer[1,2,*]

[1]*Institut für Theoretische Physik (T39), Physik-Department, Technische Universität München, D-85747 Garching, Germany*
[2]*Center for Nuclear Studies, Department of Physics, The George Washington University, Washington DC 20052, USA*
(Received 13 March 2008; published 11 June 2008)

In view of its relation to Big Bang nucleosynthesis and a reported discrepancy between nuclear models and data taken at S-DALINAC, electro-induced deuteron breakup ^{2}H$(e, e'p)n$ is studied at momentum transfer $q <$ 100 MeV and close to threshold in the low-energy nuclear effective field theory without dynamical pions, EFT($\not{\pi}$). The result at next-to-next-to-leading order (N^{2}LO) for electric dipole currents and at next-to-leading order (NLO) for magnetic ones converges order-by-order better than quantitatively predicted and contains no free parameter. It is at this order determined by simple, well-known observables. Decomposing the triple differential cross section into the longitudinal-plus-transverse ($L + T$), transverse-transverse (TT), and longitudinal-transverse interference (LT) terms, we find excellent agreement with a potential-model calculation by Arenhövel and co-workers, based on the Bonn potential. Theory and data also agree well on σ_{L+T}. There is however no space on the theory side for the discrepancy of up to 30%(3σ) between theory and experiment in σ_{LT}. From universality of EFT($\not{\pi}$), we conclude that no theoretical approach with the correct deuteron asymptotic wave function can explain the data. Undetermined short-distance contributions that could affect σ_{LT} enter only at high orders (i.e., at the few-percent level). We notice some issues with the kinematics and normalization of the data reported.

I. INTRODUCTION

The deuteron is the simplest nucleus, playing the same fundamental role in nuclear physics as the hydrogen atom in atomic physics. Its electromagnetic properties have been studied in great detail both theoretically and experimentally—among others in photodisintegration (see, e.g., Refs. [1,2] for reviews) and electrodisintegration (see, e.g., Refs. [3,4] and references therein). The latter process has the advantage of allowing for an independent variation of energy and momentum transfer. Most experiments have been performed at higher energy transfers and are in good agreement with potential-model calculations. However, one experiment [5,6] at the S-DALINAC accelerator of TU Darmstadt (Germany) examined in 2002 the triple-differential cross section for $d(e, e'p)n$ at low momentum transfer (<60 MeV/c) and close to the breakup threshold, concentrating on the decomposition into the different structure functions. For the longitudinal-transverse interference cross section σ_{LT}, a discrepancy of about 30% or up to three standard deviations was discovered relative to the prediction by Arenhövel and co-workers [4,5,7]. As the discrepancy is less pronounced with increasing momentum and energy transfer, this does not necessarily contradict other experiments at higher transfers, which are in good agreement with the same potential-model calculations (see, e.g., Ref. [8]).

The disagreement raises however a serious question: The same reaction at the real-photon point (i.e., photo-induced low-energy deuteron breakup and recombination, $np \leftrightarrow d\gamma$) is the first and very sensitive step in Big Bang nucleosynthesis (BBN). Indeed, both the higher energy regime of BBN-relevant

photodissociation and the S-DALINAC experiment on electrodissociation are most sensitive to the same electric dipole transition amplitude $E1_V$. Because of the great difficulty of performing very low energy experiments, the lack of data for this reaction in the BBN-relevant energy region $E \in [20; 300]$ keV makes nuclear theory at present the sole provider of input for the BBN network codes [9,10]. While this has also triggered further experiments at S-DALINAC [11] and the High-Intensity γ-ray Facility HIγS at TUNL [12,13], the accuracy claimed by theoretical approaches [1,14–16] is not yet matched. In view of this, the S-DALINAC findings are the more troubling: How well does theory understand the simplest nucleus at low energies, if one of the conceptually simplest nontrivial processes seems to disagree with data? Does this reflect deficits in our understanding of the long-range NN force, meson-exchange currents, "off-shell effects" and cutoff dependence, or even gauge invariance? The analysis in Ref. [5] notes that the potential-model approach "without meson-exchange, isobar and relativistic currents accounts for 99% of the final result for σ_{LT}, leaving no room for further improvement" and continues: "At present, there exists no explanation of this surprising result in the framework of conventional nuclear theory. It is an open question whether an alternative interpretation can be offered by effective field theory ...." In this work, we answer this question by concluding that *no consistent theoretical approach* can accommodate the data of Ref. [5].

We employ pion-less effective field theory EFT($\not{\pi}$) in the variant in which the effective range is re-summed into the two-nucleon propagator [17–23]. EFT($\not{\pi}$) is well tested in low-energy reactions with up to three nucleons (see, e.g., Refs. [24–27] for reviews). Even properties of ^{4}He [28–30] and ^{6}Li [31] are now studied successfully. In particular, $np \rightarrow d\gamma$ was studied because of its relevance for BBN [15,32,33], culminating in a N^{4}LO calculation by Rupak [14] with a

_____
*Corresponding author: hgrie@gwu.edu; permanent address: Center for Nuclear Studies, Department of Physics, The George Washington University, Washington DC 20052, USA.

theoretical accuracy of <1%. We here study the S-DALINAC data [5] within the same framework, noting that the lowest energy data show the biggest discrepancy and lie well within the range of applicability of EFT($\not\pi$). At momenta below the pion mass, probes cannot resolve the long-range part of the NN potential as nonlocal. Thus, the most general Lagrangean compatible with the symmetries of QCD can be built out of contact interactions between nucleons as the only dynamical effective hadronic low-energy degrees of freedom. EFT($\not\pi$) is the unique low-energy version of QCD and allows often (as in this case) for simple, closed-form results. The amplitude is expanded in a small, dimensionless parameter $Q = \frac{p_{\text{typ}}}{\Lambda_{\not\pi}}$: the ratio between a typical low-momentum scale p_{typ} of the process involved and the breakdown scale $\Lambda_{\not\pi}$, set by the mass m_π of the pion as the lightest particle not included as a dynamical effective degree of freedom. This allows one to estimate the theoretical uncertainties induced by neglecting higher order terms in the momentum expansion of all forces. With a typical low-momentum scale set by the inverse deuteron size, one obtains $Q \approx \frac{1}{3}$. Looking at the order-by-order convergence of all applications considered so far, one finds this estimate to be quite conservative and the actual convergence pattern to be much better. Dimensional regularization is employed in the two-nucleon system to renormalize high-momentum parts of loops, preserving all symmetries at each step. External currents and relativistic effects are included in a systematic, manifestly gauge-invariant way. No ambiguities arise from meson-exchange currents or off-shell effects.

The presentation is organized as follows: After recalling the essentials of EFT($\not\pi$) in Sec. II, we give the cross section and individual contributions for deuteron electrodisintegration up to next-to-next-to-leading order (N^{2}LO) for electric dipole transitions $E1_V$ and up to next-to-leading order (NLO) for magnetic isovector dipole transitions $M1_V$. Section III contains the detailed comparison with data, focusing on kinematics in the experiment (Sec. III A), the full cross section (Sec. III B) and its decomposition into the structure functions (Sec. III C), data normalization (Sec. III D), and possible higher order effects (Sec. III E). After an experiment at slightly higher energies [8] is discussed in Sec. III F, the conclusions of Sec. IV are followed by an Appendix with some useful loop integrals and the explicit form of the hadronic matrix elements. Further background and details are available in S. Christlmeier's Diplom thesis [34].

II. FRAMEWORK AND CALCULATION

A. Kinematics and cross section

The kinematic variables of the disintegration process $d(e, e'p)n$ are illustrated in Fig. 1. Two frames of reference are conventionally used (see, e.g., Refs. [3,4,35]).

On the one hand, the leptonic part $e \to \gamma^* e'$ of the process is conveniently discussed in terms of variables in the laboratory frame (the deuteron rest frame), denoted by the superscript "lab." The four-momenta are $(E_0^{\text{lab}}, \vec{k}^{\text{lab}})$ for incoming and $(E_e^{\text{lab}}, \vec{k}'^{\text{lab}})$ for outgoing electrons. The scattering angle be-
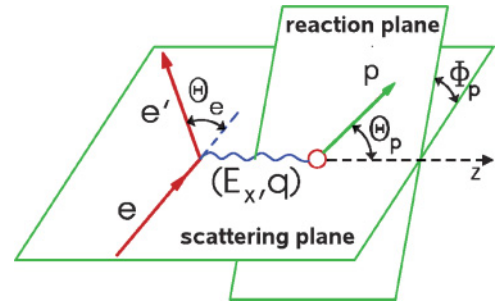
FIG. 1. (Color online) Kinematics of deuteron electrodisintegration, reproduced with the kind permission of the authors of Ref. [5]. The electron kinematics refers to the laboratory frame, while the proton variables are defined in the center-of-mass frame of the two-nucleon final state.

tween the momenta $\vec{k}^{\text{lab}}$ and $\vec{k}'^{\text{lab}}$ of the incoming and outgoing electron is Θ_e^{lab}. The energy and momentum transfer of the virtual photon is

$$E_X^{\text{lab}} := \omega^{\text{lab}} = E_0^{\text{lab}} - E_e^{\text{lab}}, \quad \vec{q}^{\,\text{lab}} = \vec{k}^{\text{lab}} - \vec{k}'^{\text{lab}}. \quad (2.1)$$

The hadronic part of the process, $\gamma^* d \to pn$, is on the other hand more conveniently calculated in its own rest frame (i.e., in the *center-of-mass frame of the outgoing nucleons* and thus of the virtual photon and deuteron). Variables in this frame carry no superscript. The outgoing proton (neutron) has momentum $\vec{p}(-\vec{p})$ and kinetic energy $\frac{p^2}{2M}$, $p := |\vec{p}|$. The scattering angles in this system are defined by $\vec{p} \cdot \vec{q} = pq \cos \Theta_p$ and $\vec{p} \cdot (\vec{q} \times \vec{k}) \propto \sin \Phi_p$. Thus, Θ_p is the angle between the virtual photon and the proton, and Φ_p is the angle between the scattering plane, spanned by the incoming and outgoing electron momenta, and the reaction plane, spanned by the proton and photon momenta.

A boost along the momentum transfer $\vec{q}$ transforms between the two frames:

$$\beta = \frac{q^{\text{lab}}}{M_d + \omega^{\text{lab}}}, \quad \gamma = \frac{1}{\sqrt{1 - \beta^2}}, \quad (2.2)$$

where $M_d = 2M - B$ is the deuteron mass. Hence, the quantities defined in the laboratory frame in Eq. (2.1) transform to the proton-neutron c.m. frame as

$$\omega = \gamma \omega^{\text{lab}} - \beta \gamma q^{\text{lab}}, \quad q = \beta \gamma M_d. \quad (2.3)$$

We choose as the five independent variables of this process the energies E_0^{lab} and E_e^{lab} (or, equivalently, $E_X^{\text{lab}} = E_0^{\text{lab}} - E_e^{\text{lab}}$) and the scattering angle Θ_e^{lab} of the electrons in the laboratory frame, plus the proton emission angles Θ_p and Φ_p in the proton-neutron c.m. frame. The momentum of the outgoing proton is

$$p = \sqrt{(\omega - B)M + q^2 \frac{M}{2M_d}}. \quad (2.4)$$

The momentum vectors are therefore parametrized such that $\vec{q}$ defines the z-direction:

$$\vec{q}^{\,\text{lab}} = (0, 0, 1)q^{\text{lab}}, \quad (2.5)$$

$$\vec{q} = (0, 0, 1)q, \quad (2.6)$$

$$\vec{k}^{\text{lab}} = \left(\sin \Theta_{0q}^{\text{lab}}, 0, \cos \Theta_{0q}^{\text{lab}} \right) k^{\text{lab}}, \quad (2.7)$$

$$\vec{k}'^{\text{lab}} = \left(\sin \Theta_{eq}^{\text{lab}}, 0, \cos \Theta_{eq}^{\text{lab}} \right) k'^{\text{lab}}, \quad (2.8)$$

$$\vec{p} = (\sin \Theta_p \cos \Phi_p, \sin \Theta_p \sin \Phi_p, \cos \Theta_p) p, \quad (2.9)$$

with the angles between the photon and the incoming or outgoing electrons translating as

$$\cos \Theta_{0q}^{\text{lab}} = \frac{k^{\text{lab}} - k'^{\text{lab}} \cos \Theta_e^{\text{lab}}}{q^{\text{lab}}},$$

$$\cos \Theta_{eq}^{\text{lab}} = \frac{k^{\text{lab}} \cos \Theta_e^{\text{lab}} - k'^{\text{lab}}}{q^{\text{lab}}}. \quad (2.10)$$

Since the transformation between these two frames is given by a boost along $\vec{q}$, it does not affect the azimuthal angle $\Phi_p \equiv \Phi_p^{\text{lab}}$.

The electron momenta are $\vec{k}_{\text{lab}}^2 = E_{0\,\text{lab}}^2 - m_e^2$ and $\vec{k}_{\text{lab}}'^2 = E_{e\,\text{lab}}^2 - m_e^2$. Although the electron mass $m_e = 0.511$ MeV does not play a role for the experiment at hand, we keep in mind applications to corners of phase space where its effects could be felt (e.g., in back-scattering [11]).

The triple-differential cross section is then derived from the amplitude $\mathcal{A}$:

$$\frac{d^3 \sigma}{dE_e^{\text{lab}} d\Omega_e^{\text{lab}} d\Omega_p}$$

$$= \frac{k'^{\text{lab}} p M_d M^2}{8(2\pi)^5 \left(M + \frac{p^2}{2M} \right) \sqrt{\left(M_d E_0^{\text{lab}} + \vec{q}^{\,\text{lab}} \cdot \vec{k}^{\text{lab}} \right)^2 - M_d^2 m_e^2}} |\mathcal{A}|^2$$

$$(2.11)$$

$$= \frac{d^3}{dE_e^{\text{lab}} d\Omega_e^{\text{lab}} d\Omega_p} (\sigma_L + \sigma_T + \sigma_{LT} \cos \Phi_p + \sigma_{TT} \cos 2\Phi_p),$$

$$(2.12)$$

where the spherical angles are $\Omega_e^{\text{lab}} = (\Theta_e^{\text{lab}}, \Phi_e^{\text{lab}} \equiv 0)$ and $\Omega_p = (\Theta_p, \Phi_p)$. In the second line, the dependence on the azimuthal proton emission angle Φ_p is decomposed into the longitudinal-plus-transverse parts $\sigma_L + \sigma_T$ and the interference terms σ_{LT} and σ_{TT} [3,4,35]. For any process to contribute to either of the interference terms, it must from Eq. (2.9) depend on those components of the outgoing proton momentum $\vec{p}$ that are transverse to the photon momentum $\vec{q}$. This will become important in the analysis later.

The scattering amplitude $\mathcal{A}$ is rewritten in terms of the photon propagator $D_{\mu\nu}^{(\gamma)}$, the hadronic current J_{hadr}^μ to be calculated in EFT($\not{\pi}$) in the following, and the leptonic current l_μ whose contribution to lowest order in the fine-structure constant is easily found:

$$\mathcal{A} = l^\mu D_{\mu\nu}^{(\gamma)} J_{\text{hadr}}^\nu. \quad (2.13)$$

Current conservation implies $q_\mu l^\mu = 0 = q_\mu J_{\text{hadr}}^\mu$ and is at this order in the fine-structure constant α equivalent to gauge invariance.

If the variables of Ref. [5] are interpreted as discussed in Sec. III A, the S-DALINAC experiment was performed at two sets of incident electron energies $E_0^{\text{lab}} \in \{50; 85\}$ MeV, a range of photon energies $E_X^{\text{lab}} \in [8; 16]$ MeV, electron scattering angle $\Theta_e^{\text{lab}} = 40°$, and azimuthal angle $\Phi_p = 45°$. This leads to photon momentum transfers $q \in [32; 65]$ MeV and outgoing

proton momenta $p \in [74; 106]$ MeV in the proton-neutron c.m. frame. These are the relevant external low-momentum scales of the hadronic matrix element.

B. Lagrangean and parameter fixing

EFT($\not{\pi}$) allows one to address the questions raised by the S-DALINAC data in a model-independent, systematic setting with a reliable estimate of the theoretical uncertainties, free of ambiguities, such as off-shell effects and cutoff dependence. As the parts of the effective Lagrangean of EFT($\not{\pi}$), its power-counting rules, and the parameter fixing necessary for this work have been discussed extensively by Beane and Savage [22], we repeat them here only briefly. The Feynman rules are also given in Ref. [34] Appendix A. The Lagrangeans are

$$\mathcal{L}_N = N^\dagger \left[iD_0 + \frac{\vec{D}^2}{2M} + \frac{e}{2M} (\kappa_0 + \kappa_1 \tau_3) \vec{\sigma} \cdot \vec{B} \right] N, \quad (2.14)$$

$$\mathcal{L}_s = -s_a^\dagger \left[iD_0 + \frac{\vec{D}^2}{4M} - \Delta_s \right] s_a - y_s \left[s_a^\dagger N^T P_a^{(^1S_0)} N + \text{H.c.} \right], \quad (2.15)$$

$$\mathcal{L}_t = -t_i^\dagger \left[iD_0 + \frac{\vec{D}^2}{4M} - \Delta_t \right] t_i - y_t \left[t_i^\dagger N^T P_i^{(^3S_1)} N + \text{H.c.} \right]$$

$$- \frac{C_{sd}}{\sqrt{M \rho_d}} \left[\delta_{ix} \delta_{jy} - \frac{1}{3} \delta_{ij} \delta_{xy} \right] [t_i^\dagger (N^T \mathcal{O}_{xy,j} N)] + \text{H.c.}$$

$$- \frac{C_Q}{M \rho_d} t_i^\dagger [iD_0, \mathcal{O}_{ij}] t_j, \quad (2.16)$$

$$\mathcal{L}_{\text{st}} = \frac{e L_1}{M \sqrt{r_0 \rho_d}} [t_i^\dagger s_3 B_i + \text{H.c.}]. \quad (2.17)$$

The one-nucleon Lagrangean $\mathcal{L}_N$ of the nucleon isodoublet $N = \binom{p}{n}$ with isospin-averaged mass $M = 938.9$ MeV consists of two parts: the kinetic term with minimal substitution, $D_\mu = \partial_\mu + ieQA_\mu$, where $Q = \frac{1}{2}(1 + \tau_3)$ is the nucleon charge matrix and $\alpha = \frac{e^2}{4\pi} = \frac{1}{137}$ the fine-structure constant, and the interaction via the isoscalar (isovector) magnetic moments, $\kappa_0 = 0.44 (\kappa_1 = 2.35)$ in nuclear magnetons. The spin (isospin) Pauli matrices with vector (isovector) index $i = 1, 2, 3 (a = 1, 2, 3)$ are denoted by $\sigma_i (\tau_a)$.

The Lagrangean for the auxiliary dibaryon field $s_a(t_i)$ in the $^1S_0(^3S_1)$ channel is $\mathcal{L}_s(\mathcal{L}_t)$ [17–19]. (In EFT, this was first considered in Ref. [36].) As we probe only the np system, $D_\mu = \partial_\mu + ieA_\mu$ for both dibaryons. The projection operators are $P_a^{(^1S_0)} = \frac{1}{\sqrt{8}} \sigma_2 \tau_2 \tau_a$, $P_i^{(^3S_1)} = \frac{1}{\sqrt{8}} \sigma_2 \sigma_i \tau_2$. The auxiliary-field parameters are matched to the effective-range expansion of NN scattering such that the effective range is re-summed to all powers to speed up convergence and simplify calculations of some higher order effects [17–23]:

$$y_s = \frac{\sqrt{8\pi}}{M\sqrt{r_0}}, \quad \Delta_s = \frac{2}{Mr_0} \left(\frac{1}{a_0} - \mu \right), \quad y_t = \frac{\sqrt{8\pi}}{M\sqrt{\rho_d}},$$

$$\Delta_t = \frac{2}{M\rho_d} \left(\gamma - \frac{\rho_d}{2} \gamma^2 - \mu \right). \quad (2.18)$$

The parameter μ encodes the linear cutoff divergence of individual diagrams, calculated in the power-divergence

subtraction (PDS) scheme version of dimensional regularization [37,38]. It is imperative for self-consistency that physical amplitudes are independent of μ. This is indeed the case.

For the spin-singlet, the scattering length and effective range of the np system are probed in deuteron electrodisintegration: $a_0 = -23.71$ fm, $r_0 = 2.73$ fm. Parameters for the spin-triplet are determined from the effective-range expansion about the observed real bound state, namely the deuteron with binding energy $B = 2.225$ MeV (corresponding to a momentum $\gamma = \sqrt{MB} = 45.70$ MeV) and effective range $\rho_d = 1.764$ fm. Therefore, the deuteron wave function shows the correct exponential decay and normalization Z already at leading order (LO) in EFT($\not\!\pi$) [22,39]:

$$\Psi_{\text{deuteron}}(r \to \infty) = \sqrt{\frac{Z}{2\pi\rho_d}}\frac{e^{-\gamma r}}{r} \quad \text{with} \quad Z = \frac{\gamma\rho_d}{1-\gamma\rho_d}. \tag{2.19}$$

The last two terms of $\mathcal{L}_t$ parametrize SD-wave mixing in the spin-triplet, with

$$\mathcal{O}_{xy,j} = -\tfrac{1}{4}\big(\overleftarrow{D}_x\,\overleftarrow{D}_y P_j^{(3S_1)} + P_j^{(3S_1)}\,\overrightarrow{D}_x\,\overrightarrow{D}_y$$
$$-\,\overleftarrow{D}_x P_j^{(3S_1)}\,\overrightarrow{D}_y - \overleftarrow{D}_y P_j^{(3S_1)}\,\overrightarrow{D}_x\big), \tag{2.20}$$

$$\mathcal{O}_{ij} = -\big(\vec{D}_i\vec{D}_j - \tfrac{1}{3}\delta_{ij}\vec{D}^2\big) \tag{2.21}$$

operators, which ensure that $\mathcal{L}_{\text{st}}$ is manifestly gauge invariant. Their strengths are determined from the asymptotic ratio $\eta_{sd} = 0.0254$ of D- and S-wave components of the deuteron wave function and of the deuteron quadrupole moment $\mu_Q = 0.2859$ fm^2 [22]:

$$C_{sd} = \frac{6\sqrt{\pi}\eta_{sd}}{\sqrt{M}\gamma^2}, \quad \mu_Q = 2Z\left[y_t\frac{C_{sd}}{\sqrt{M\rho_d}}\frac{M^2}{32\pi}\frac{2}{3\gamma} + \frac{C_Q}{M\rho_d}\right]. \tag{2.22}$$

Here, C_{sd} contributes at LO, and C_Q provides a NLO correction of about 50%.

Finally, $\mathcal{L}_{\text{st}}$ in Eq. (2.17) parametrizes transitions between the $^1S_0$ and $^3S_1$ channels by a magnetic field acting on a dibaryon. Its strength is determined by the thermal cross section $\sigma(E = \frac{p^2}{M} = 1.264 \times 10^{-8}$ MeV$) = (334.2 \pm 0.5)$ mb [40] for radiative capture of neutrons on protons, $np \to d\gamma$. At thermal energies, it is dominated by isovectorial $M1_V$ transitions. Magnetic moment interactions are LO, and the parameter L_1 in $\mathcal{L}_{\text{st}}$ enters as a NLO correction of about 50%, whereas electric transitions are irrelevant. The free parameter is thus determined from the thermal cross section [22]

$$\sigma^{(M1_V)} = \frac{2\alpha Z(p^2 + \gamma^2)^3}{pM^3}\left|\frac{1}{-\frac{1}{a} + \frac{1}{2}r_0 p^2 - ip}\right|^2$$
$$\times\left[\kappa_1\frac{\gamma - \frac{1}{a} + \frac{1}{2}r_0 p^2}{p^2 + \gamma^2} + \frac{L_1}{2}\right]^2 \tag{2.23}$$

as $L_1 = -4.41$ fm [34] or $L_1 = -4.0$ fm [22], depending on whether terms quadratic in L_1 are kept. Both variants differ by $10\% \lesssim Q$, as expected from L_1 being a higher order correction.

We now state the power-counting rules of EFT($\not\!\pi$) in the version in which the effective-range parameters are treated

as unnaturally large and thus are kept at LO together with the scattering lengths [22]. The typical low-energy c.m. momentum $\vec{p}$ and kinetic energy $E/2$ of a nucleon get counted as

$$|\vec{p}| \sim \sqrt{ME} \sim \gamma \sim \frac{1}{\rho_d} \sim \frac{1}{r_0} \sim \frac{1}{a_0} \sim \mu \sim Q\Lambda_\pi. \tag{2.24}$$

Hence, the wave function renormalization scales as $Z \sim 1$. SD mixing is suppressed by Q^2 with respect to pure S-wave amplitudes because of the two derivatives in Eq. (2.16). Finally, the ratio of the isoscalar and isovector magnetic moments is $\kappa_0/\kappa_1 \approx 1/5 \lesssim Q$. Therefore, κ_0 is neglected as numerically higher order in the following [41].

Since the gauge field is minimally coupled, these rules are simple to extend: The zero component of the gauge field A_μ scales like an energy, $A^0 \sim Q^2$; its three-vector components scale like a momentum, $\vec{A} \sim Q$. As seen in the previous section, photon energies for the S-DALINAC kinematics of deuteron electrodisintegration lie in the range $E_X^{\text{lab}} \in [8;16]$ MeV, corresponding to $E_X \in [6;14]$ MeV $\sim [Q^2\Lambda_\pi^2/M; Q^2\Lambda_\pi]$, photon momenta in the range $q \in [32;65]$ MeV $\sim Q\Lambda_\pi$, and outgoing proton momenta in the range $p \in [74;106]$ MeV $\sim Q\Lambda_\pi$, approaching $\Lambda_\pi \approx m_\pi$. Convergence must therefore be checked with care.

C. Electric contributions to N²LO

Electric dipole transition amplitudes $E1_V$ dominate not only the photodissociation cross section at the higher end of the energy range relevant for BBN but also electrodisintegration for $p \gtrsim 20$ MeV. To N²LO, the hadronic currents have the structure

$$J_{\text{hadr}}^{(E1_V)\mu} = ie\sqrt{Z}\frac{1}{\sqrt{8}}(N_p^\dagger\sigma^i\sigma_2 N_n^*)\epsilon_{(d)}^j J_{ij}^\mu, \tag{2.25}$$

where the proton and neutron spinors $N_{p/n}$ are specified explicitly. The indices on the current J_{ij}^μ indicate the polarization j of the initial deuteron and the spin i of the pn-triplet final state. By averaging over spins and polarizations, the electric contribution to Eq. (2.11) is

$$|\mathcal{A}_{E1_V}|^2 = \frac{(4\pi\alpha)^2}{(\omega^2 - q^2)^2}\frac{Z}{6}\Big\{\big[k_{\text{lab}}'^\mu J_\mu^{\dagger ij}\,k_{\text{lab}}^\nu J_\nu^{ij} + (\mu \leftrightarrow \nu)\big]$$
$$-\,\big(k_\mu^{\text{lab}}k_{\text{lab}}'^\mu - m_e^2\big)J_\nu^{\dagger ij} J^{\nu ij}\Big\}. \tag{2.26}$$

The three diagrams contributing at leading order, Q^0, are shown in Fig. 2. In the last two graphs, the photon couples to the deuteron, which is at this order a pure S-wave state. These diagrams are therefore independent of the direction of
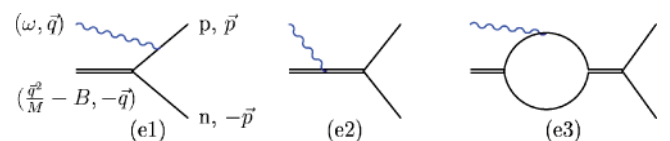
FIG. 2. (Color online) The LO electric contributions to the hadronic current. The double line denotes the spin-triplet dibaryon intermediate state. There is no NLO contribution.
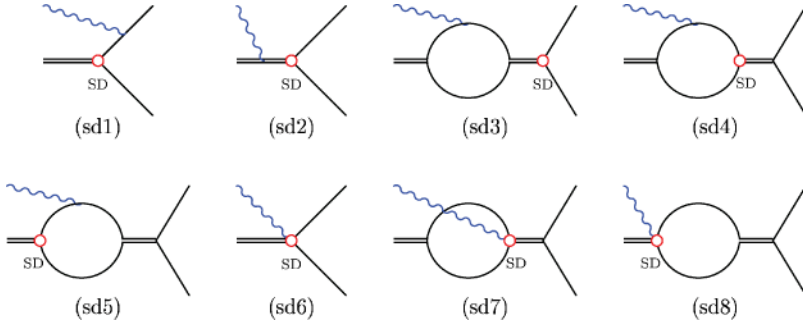
FIG. 3. (Color online) The order-Q^2 (N^{2}LO) electric contributions. The SD-mixing vertex proportional to C_{SD} is denoted by a circle; further notation as in Fig. 2.

the outgoing proton momentum $\vec{p}$ and hence via Eq. (2.9) of the proton emission angle Φ_p. They thus do not contribute to the longitudinal-transverse and transverse-transverse parts of the cross section [Eq. (2.12)]. In contradistinction, the final-state interaction in diagram (e1) depends on $\vec{p}$ and thus contributes to σ_{LT} and σ_{TT}.

There are no electric contributions at NLO. The first nonzero corrections, listed in Fig. 3, appear at N^{2}LO. All arise from SD mixing proportional to C_{SD} in the Lagrangean [Eq. (2.17)]. Relative to the LO contributions, these diagrams are suppressed by two more derivatives (i.e., two more powers of $Q \approx \frac{1}{3}$) and thus should contribute at most $(\frac{1}{3})^2 \approx 10\%$ of the LO terms. The error one makes by truncating the series at this order should be $(\frac{1}{3})^3 \approx 4\%$. The convergence is indeed much better because the asymptotic SD ratio is numerically $\eta_{sd} = 0.0254 \approx Q^3$ (i.e. N^{3}LO). Even at the S-DALINAC kinematics of photon momenta as large as 78 MeV ($E_0^{\mathrm{lab}} = 50$ MeV, $E_X^{\mathrm{lab}} = 9$ MeV, $\Theta_e^{\mathrm{lab}} = 40°$, and $\Phi_p = 45°$), they amount to not more than 1% of the total; see the discussion and figures in Secs. III B and III C as well as Ref. [34] for details. Only the diagrams (sd1-3) and (sd6) contribute to the interference terms σ_{LT} and σ_{TT} via their final-state interaction or via the D-wave component induced into the deuteron and np final-state wave function.

The resulting electric currents up to N^{2}LO are detailed in Appendix B. At each order, they are manifestly gauge invariant and cutoff independent.

D. Magnetic contributions to NLO

Magnetic dipole transitions $M1_V$ dominate the inverse reaction $np \to d\gamma$ at the lower end of the energy range relevant for BBN, but they are usually small at S-DALINAC kinematics. We therefore include them only to NLO (Fig. 4). The LO part is set by the isovector magnetic moment κ_1; the only NLO graph, (m4), comes from the singlet-triplet coupling [Eq. (2.17)].

The hadronic currents from magnetic contributions can to this order be written as

$$J_{\mathrm{hadr}}^{(M1_V)k} = e\sqrt{Z}\epsilon^{ijk}\epsilon_{(d)}^i \frac{1}{\sqrt{8}}(N_p^\dagger \sigma_2 N_n^*)\, J^j, \qquad (2.27)$$

and the squared amplitude is, after averaging over initial states,

$$\begin{aligned}
|\mathcal{A}_{M1_V}|^2 &= \frac{(4\pi\alpha)^2}{(\omega^2 - q^2)^2}\frac{Z}{6}(\delta^{jm}\delta^{kn} - \delta^{km}\delta^{jn}) \\
&\quad \times \left[k_n'^{\mathrm{lab}} J^{\dagger j}k_k^{\mathrm{lab}} J^m + k_k'^{\mathrm{lab}} J^m k_n^{\mathrm{lab}} J^{\dagger j}\right. \\
&\quad \left. + (k_\mu^{\mathrm{lab}} k'^{\mathrm{lab}\mu} - m_e^2)J^{\dagger j}J^m\delta^{kn}\right].
\end{aligned} \qquad (2.28)$$

The vertex where a magnetic photon couples to a dibaryon largely reduces the amplitude, although it is formally NLO. Compared to the electric amplitude, the magnetic one is suppressed by two orders of magnitude in the energy regime of the S-DALINAC experiment, except for the vicinity of $\Theta_p = 70°$; see Figs. 5 to 8.

It is not too difficult to see that the only angular dependence in the magnetic amplitude comes from the $\vec{p} \cdot \vec{q}$ terms in the intermediate nucleon propagators, as the deuteron and outgoing np system are again pure S states in these diagrams. Thus, the amplitudes only test the longitudinal part of $\vec{p}$. There is no Φ_p dependence, and therefore magnetic transitions at this order do not contribute to σ_{LT} and σ_{TT} interference terms [Eq. (2.12)].

The explicit form of the resulting magnetic currents can be found in Appendix C. At each order, they are manifestly gauge invariant and cutoff independent.

III. THEORY CONFRONTS DATA

We now compare the results of EFT($\not\pi$) to the S-DALINAC data reported in Refs. [5,6] and to the potential model calculation by H. Arenhövel and co-workers, which is based on the Bonn-C r-space potential and includes final-state effects,

FIG. 4. (Color online) The magnetic contributions to the hadronic current at LO (m1–m3) and NLO (m4). The blob denotes a magnetic photon coupling via the isovectorial magnetic moment, the square the dibaryon-photon interaction [Eq. (2.17)] proportional to L_1, and the dashed double line the spin-singlet dibaryon intermediate state; further notation as in Fig. 2.
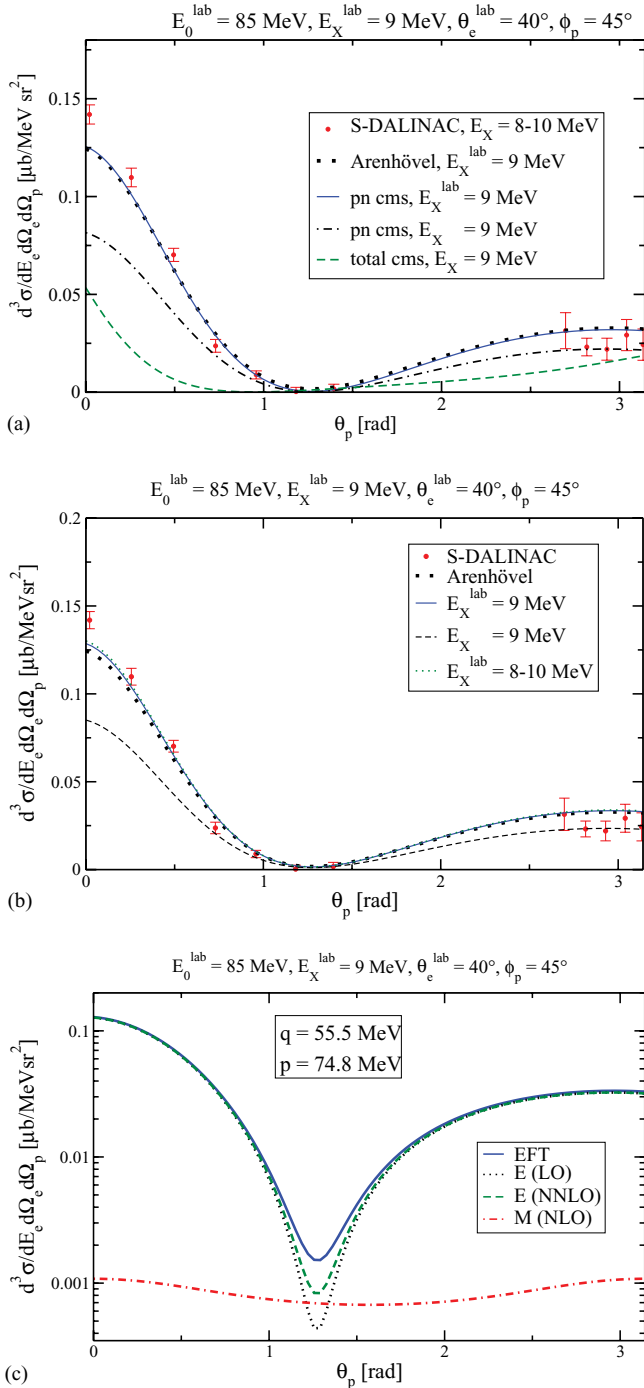
FIG. 5. (Color online) Examples of the triple-differential cross section for $E_X^{\text{lab}} = 9$ MeV at $E_0^{\text{lab}} = 85$ MeV, compared to S-DALINAC data [5] (with combined statistical and systematic error bars) and to the result by Arenhövel and co-workers [4,5,7] (squares). (a) Interpretation of "$E_X = 9$ MeV" as given in the total c.m. frame, the *pn* c.m. frame, or the laboratory frame. (b) EFT($\pi\!\!\!/$) at $E_X^{\text{lab}} = 9$ MeV (solid line) and $E_X^{(pn)-\text{c.m.}} = 9$ MeV (i.e., $E_X^{\text{lab}} = 10.6$ MeV; dashed). The dotted curve is the double-differential cross section per MeV, obtained by integrating over the bin $E_X^{\text{lab}} \in [8; 10]$ MeV; the difference from the solid line is almost invisible. (c) Comparison on a logarithmic scale of the EFT($\pi\!\!\!/$) contributions: electric transitions up to LO and N²LO, respectively (recall that NLO is zero), and magnetic transitions up to NLO.

meson-exchange currents, isobar configurations, and (in our case negligible) relativistic effects [4,5,7]. Before we consider the energy and angular dependence of the triple-differential cross section and its decomposition, we first have to address a subtle kinematical point.

A. Kinematics, again

In Sec. II A, we adopted the standard kinematics of electrodisintegration, according to which the leptonic part of the cross section is calculated in the laboratory frame (deuteron at rest), while the hadronic part is determined in the proton-neutron c.m. frame of the hadronic subprocess $\gamma^* d \to pn$. In a slight but revealing abuse of language, the latter is often referred to as "the c.m. frame." According to a literal reading of Ref. [5], the S-DALINAC experiment would have been analyzed in the center of mass frame of the *whole* process, resulting in large deviations between theory and experiment both in shape and normalization even of the full triple-differential cross section (see Fig. 5). We take this to be a slip of the tongue and assume that the experiment was analyzed by using standard kinematics [3,4,35].

Furthermore, the variable that labels the energy transferred by the photon in the S-DALINAC experiment is said to be obtained "after transformation to the center-of-mass system" [5]. However, agreement of the data with both the potential-model and EFT($\pi\!\!\!/$) calculation is found only if the S-DALINAC variable "E_X" refers to the laboratory frame. The point $E_X^{(pn)-\text{c.m.}} = 9$ MeV would correspond to $E_X^{\text{lab}} = 10.6$ MeV and a much smaller cross section, so that the resulting curve would again substantially deviate from data (see Fig. 5). We therefore interpret "E_X" in [5] as E_X^{lab}, defined in the rest frame of the deuteron target.

The experimental results are reported in four energy bins, $E_X^{\text{lab}} = [8; 10], [10; 12], [12; 14],$ and $[14; 16]$ MeV. We interpret them such that the count rate was normalized to give the double-differential cross section per MeV. Thus, we compare the triple-differential cross section for E_X^{lab} to the double-differential one *per MeV*. The difference between averaging over the 2-MeV range and taking the mean value of E_X^{lab} can be neglected down to $E_X^{\text{lab}} = 6$ MeV, as shown in the plot; see also Ref. [34]. If E_X is interpreted as given in the *pn* c.m. frame *and* the cross section as given over the whole 2-MeV bin, the data would consistently overshoot the theory results by 10% to 20%.

We are grateful to H. Arenhövel [7] for confirming that the potential-model results reported in Ref. [5] were determined in the same kinematics used here.

B. Total differential cross section

Comparing in Fig. 6 the differential cross sections reported in Ref. [5] at $E_0^{\text{lab}} = 50$ and 85 MeV in several E_X^{lab} bins confirms our interpretation of the experiment's kinematical variables. At $E_0^{\text{lab}} = 85$ MeV, additional data at large Θ_p are available and within their (combined statistical and systematic) error bars these are compatible with both theoretical approaches. We note excellent agreement with the
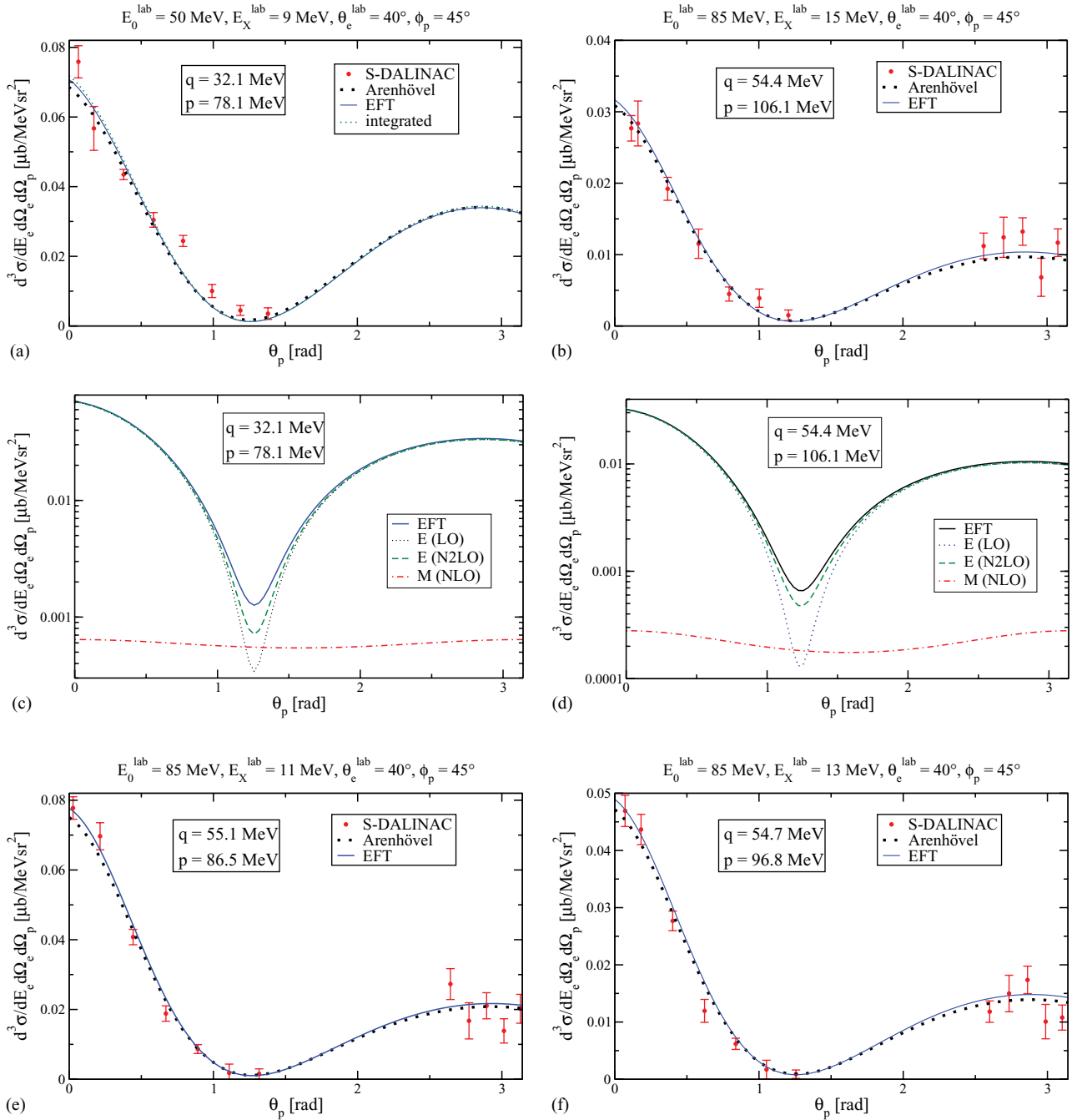
FIG. 6. (Color online) EFT($\not{\pi}$) results for the differential cross section, compared to data and calculations by Arenhövel and co-workers. (a) Data set at smallest energy and momentum transfer: $E_0^{\text{lab}} = 50$ MeV, $E_X^{\text{lab}} = 9$ MeV. (b) Data sets at largest energy and momentum transfer: $E_0^{\text{lab}} = 85$ MeV, $E_X^{\text{lab}} = 15$ MeV. (e), (f) Data set at $E_0^{\text{lab}} = 85$ MeV, $E_X^{\text{lab}} = \{11; 13\}$ MeV. Comparisons of EFT($\not{\pi}$) contributions are in panels (c) and (d) included for the smallest and largest energy and momentum transfer: electric transitions up to LO and N^{2}LO, respectively (NLO is zero), and magnetic transitions up to NLO.

calculation by Arenhövel and co-workers and with the data within error bars. In Fig. 6, a decomposition of the different contributions in EFT($\not{\pi}$) for the smallest and the largest energy and momentum transfer of the S-DALINAC data is also shown. As expected, the LO electric transitions dominate except around the minimum at $\Theta_p \approx 70°$, where N^{2}LO contributions and magnetic transitions play a significant role. That means that by taking into account only minimal coupling of photons

to nucleon and dibaryon fields, disintegration can be described highly accurately within EFT($\not{\pi}$). SD mixing, being the only correction up to N^{2}LO, contributes even less than estimated by power counting. This good convergence confirms our confidence that our results are reliable. Less-known short-distance contributions play a very minor role (see Sec. III E).

The convergence plots also reveal an interesting facet: The N^{2}LO contribution has increased slightly for higher energy
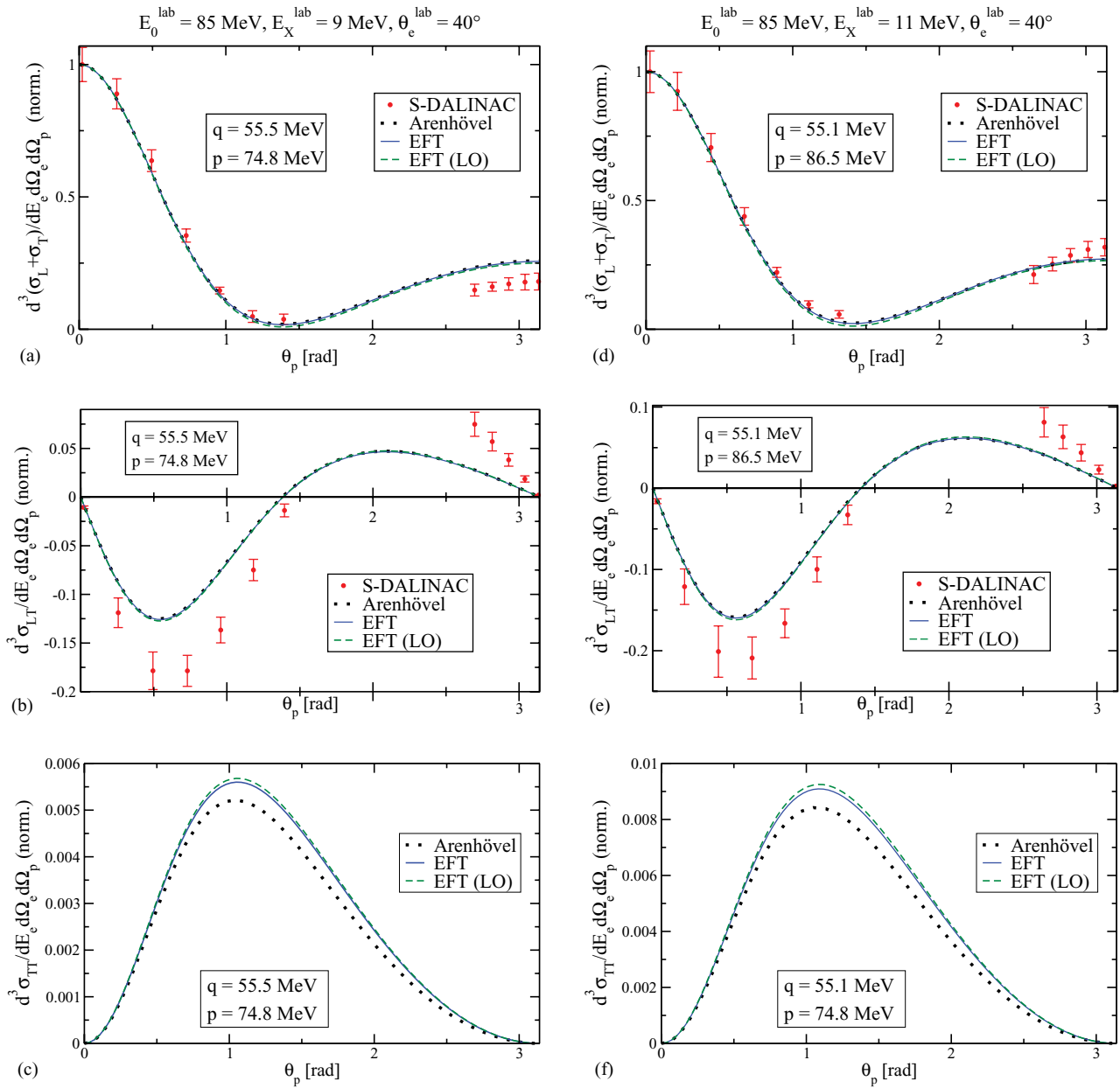
FIG. 7. (Color online) Decomposition of the triple-differential cross section into (top to bottom) longitudinal-plus-transverse ($L + T$), longitudinal-transverse (LT), and transverse-transverse (TT) parts at $E_0^{\text{lab}} = 85$ MeV, normalized to σ_{L+T} at $\Theta_p = 0$. Left column: $E_X^{\text{lab}} = 9$ MeV; right column: $E_X^{\text{lab}} = 11$ MeV. No data are available for the TT interference cross section.

and momentum transfer, but much less than expected from naive dimensional analysis. Deviations between the potential-model and EFT($\not{\pi}$) results are also slightly more pronounced there, especially at large Θ_p. As typical momenta in the process approach the breakdown scale $\Lambda_{\not{\pi}}$ of EFT($\not{\pi}$), the dimensionless parameter $Q = p_{\text{typ}}/\Lambda_{\not{\pi}}$ approaches unity and the expansion is rendered useless. The momentum transfer $q \in [32; 56]$ MeV is comparable to the intrinsic low-momentum scale of the two-nucleon system, namely the deuteron "binding momentum" $\gamma \approx 45$ MeV. The momentum of the final-state proton in the proton-neutron c.m. frame ranges however from 75 to 106 MeV and hence becomes at the upper end comparable to $\Lambda_{\not{\pi}} \approx m_\pi$. One would have expected this to

affect in particular the final-state interaction diagrams and the SD-mixing contributions at N²LO, which depend on $\vec{p}$ in the numerator. The observed enhancement is however much smaller. The good convergence of EFT($\not{\pi}$)—even for momenta close to the breakdown scale—was found also in many other applications (see, e.g., Refs. [25–27,42]).

C. Comparing structure functions

The main goal of the S-DALINAC experiment [5] was a decomposition of the contributions of different structure functions in Eq. (2.12): the longitudinal-plus-transverse cross
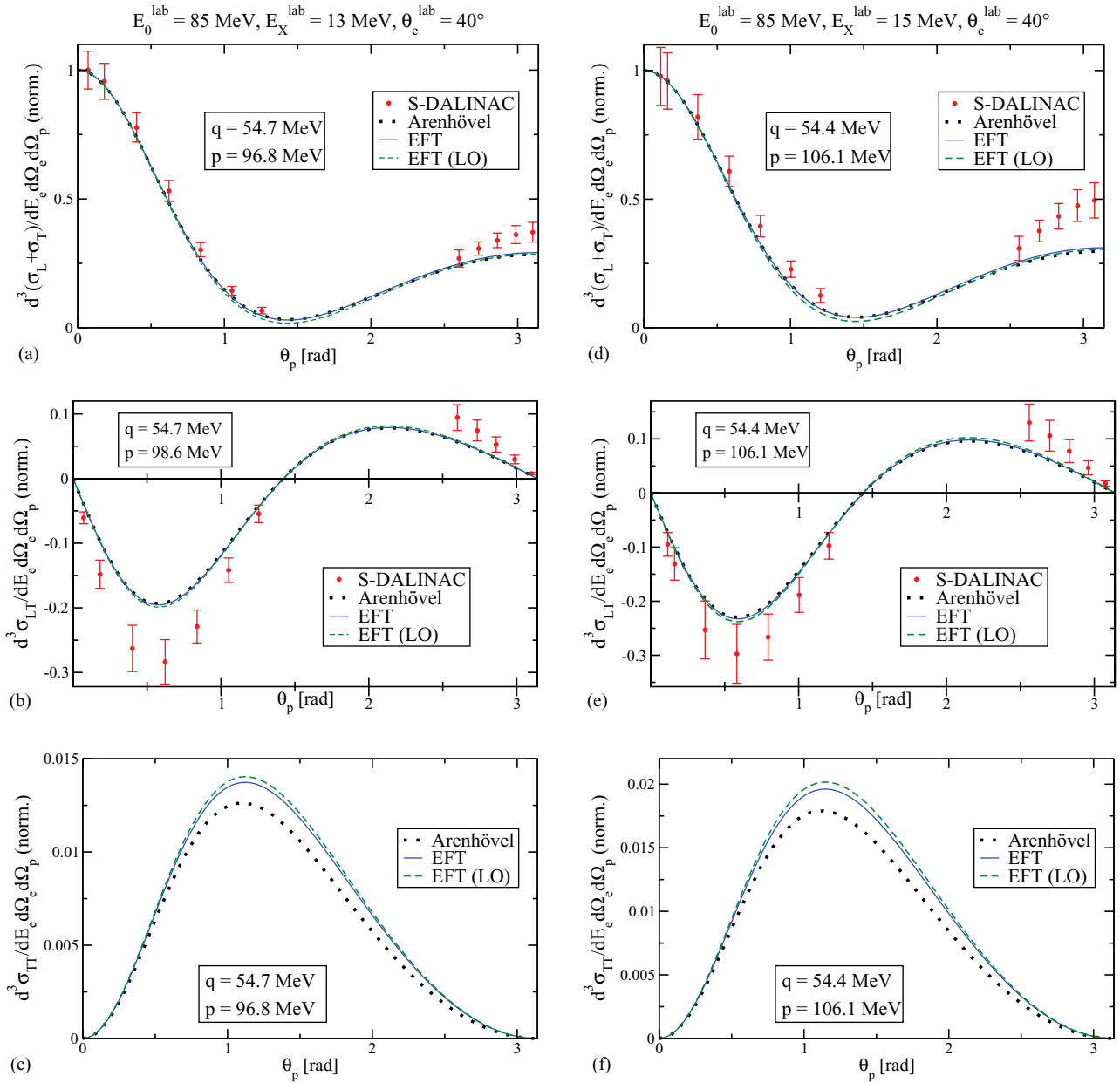
FIG. 8. (Color online) The same as Fig. 7, but for $E_X^{lab} = 13$ MeV (left column) and $E_X^{lab} = 15$ MeV (right column).

section and the LT- and TT-interference parts. However, the uncertainties in the data turned out to be too large for a meaningful comparison of σ_{TT} to theory. Studying the interference terms provides information about the impact of final-state interactions, since these can be Φ_p dependent, as reiterated in Sec. II A. The contributions of the $L + T$, LT, and TT terms are shown in Figs. 7 and 8 for $E_0^{lab} = 85$ MeV and $E_X^{lab} = \{9; 11; 13; 15\}$ MeV, again compared to data and the potential-model result.

The results are normalized to $d^3(\sigma_L + \sigma_T)/(dE_e^{lab} d\Omega_e^{lab} d\Omega_p)$ at $\Theta_p = 0°$ to make the comparison independent of the absolute normalization of the data. This also mutes the question of whether the cross sections were averaged or summed over each E_X^{lab} bin. The error of the value to which

the data are normalized has been taken into account in all error bars. One sees that $\sigma_L + \sigma_T$ dominates, whereas σ_{LT} and σ_{TT} are one and two orders of magnitude smaller, respectively. However, the interference terms become more relevant with increasing energy transfer, reflecting the growing impact of final-state interactions. In each figure, the result for the LO electric transitions in EFT($\not\pi$) is also given. Recall that, in that case, σ_{LT} and σ_{TT} are nonzero only because of the final-state interaction of the proton with the virtual photon after the deuteron breakup [Fig. 2.(e1)]. The degree to which the $E1_V$ transition dominates—already discussed in the previous section—is even more striking for σ_{LT}. Magnetic transitions do not contribute at all to the interference cross sections, since their amplitudes are independent of Φ_p (see Sec. II D). The

impact of SD mixing is increasing slightly with E_X^{lab}, but the mixing is small for $\sigma_L + \sigma_T$ and σ_{TT} and almost negligible for σ_{LT}.

The EFT($\not{\pi}$) results are again in good agreement with those of Arenhövel and co-workers, and especially σ_{LT} is essentially identical in both calculations. Only in the very small quantity σ_{TT} can a deviation be detected. It is a factor of 4 larger than the difference between the LO and N^{2}LO results, which in turn is one way to estimate higher order effects. However, we already hinted that the contributions from SD mixing and magnetic moment interactions are much smaller than estimated by naive power counting. Another estimate for possible corrections is to set the uncertainty of the EFT($\not{\pi}$) calculation at N^{2}LO as $\sim Q^3 = (p_{\mathrm{typ}}/\Lambda_\pi)^3 \approx [3\dots 10]\%$ of the LO term, by assuming a typical momentum $p_{\mathrm{typ}} \sim q \approx [45;60]$ MeV. This is apt to overestimate the theoretical uncertainties, as discussed in Sec. III E in conjunction with possible higher order corrections. In short, all EFT($\not{\pi}$) results should be understood with an uncertainty that reflects an estimate of the higher order effects not considered. A conservative accuracy limit would be $\lesssim 10\%$ in each observable. It is thus safe to conclude that the potential-model and EFT($\not{\pi}$) results agree within the theoretical uncertainties.

D. How to resolve discrepancies with data?

The accordance of both theoretical approaches with the data, however, is considerably worse. The discrepancy ranges from just over one standard deviation at the largest energy and momentum transfer to three and more at the smallest energy and momentum transfer. Not only does the calculated longitudinal-transverse interference cross section deviate by about 30% from the measured one (as pointed out in Ref. [5]), but so does $\sigma_L + \sigma_T$ at large Θ_p. In particular, it is remarkable that the latter is overpredicted at $E_X^{\mathrm{lab}} = 9$ MeV but underpredicted at $E_X^{\mathrm{lab}} = 15$ MeV. A look at $\sigma_L + \sigma_T$ at $\Theta_p = 180°$ *before data normalization* reveals however a reduced discrepancy (see Fig. 9). Only then do data and theory agree on the shape of the curve, except at the smallest value of E_X^{lab}, and an additional normalization would solve the problem. Although the statistical significance of the discrepancy hardly changes, this may indicate unaccounted systematic errors in the data.

Normalizing to $\Theta_p = 0$ seems to deteriorate the accord of calculations and data, although it avoids accounting for the absolute normalization of data. The reason can be seen by comparing Figs. 9(b) and 9(c): The cross sections both at $\Theta_p = 0$ and $\Theta_p = 180°$ display relatively small deviations, which go, however, in different directions: The theoretical result (e.g., at $E_X^{\mathrm{lab}} = 15$ MeV) is a bit too small for $\Theta_p = 180°$, but it is too large for $\Theta_p = 0$. In dividing these two values, the discrepancy increases.

The significant difference between data on the one hand and the agreeing theoretical predictions of EFT($\not{\pi}$) and Arenhövel and co-workers on the other continues for the longitudinal-transverse interference cross section σ_{LT} [see Figs. 7(b) and 7(e) and 8(b) and 8(e)]. The angular dependence of the normalized values is reproduced, but the normalization differs
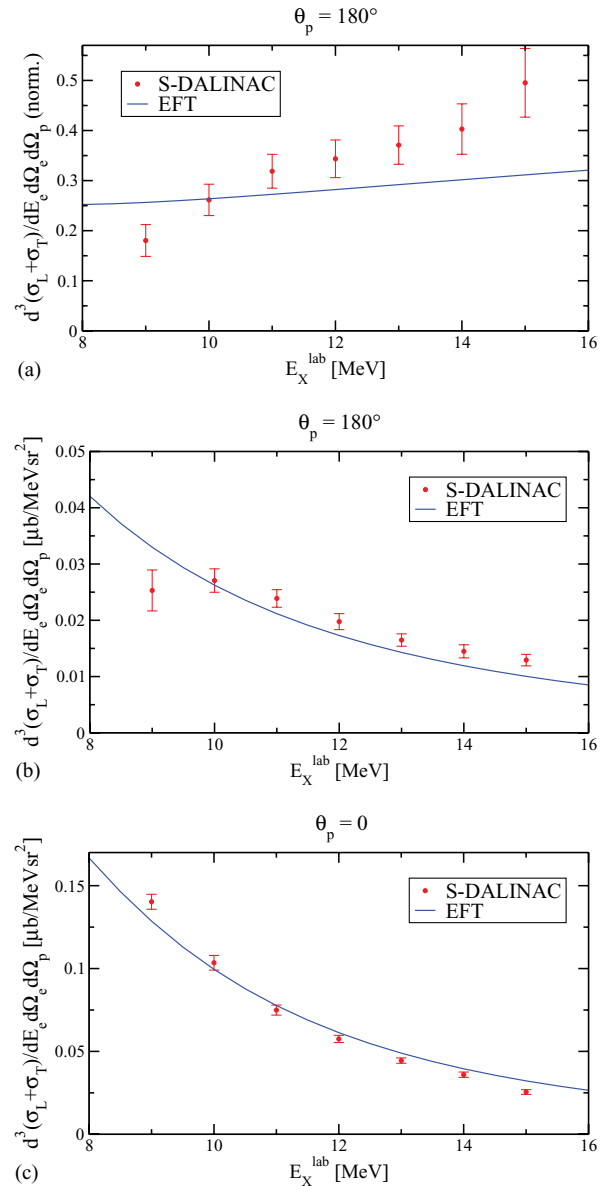
FIG. 9. (Color online) E_X^{lab} dependence of $\sigma_L + \sigma_T$ at $\Theta_p = 180°$, normalized to $\Theta_p = 0°$ (a) and before normalization (b), and (c) $\sigma_L + \sigma_T$ at $\Theta_p = 0°$ (to which all data are normalized). All graphs refer to $E_0^{\mathrm{lab}} = 85$ MeV, $\Theta_e^{\mathrm{lab}} = 40°$.

between one standard deviation at high energy and momentum transfer and three standard deviations at high energy and momentum transfer.

Figure 10 examines the energy dependence of the discrepancy for σ_{LT} at the minimum around $\Theta_p = 35°$ as a function of E_X^{lab}, both before and after normalization of the data. Again, the situation becomes, at least for higher energies, slightly better when one looks at the absolute values. However, a clear deviation remains, and it surprisingly becomes larger at smaller E_X^{lab}. The shapes and slopes of the un-normalized energy dependence of the minima in σ_{LT} do not match. The un-normalized data at high energy are, at least at non-backward angles, compatible with the theoretical approaches within error
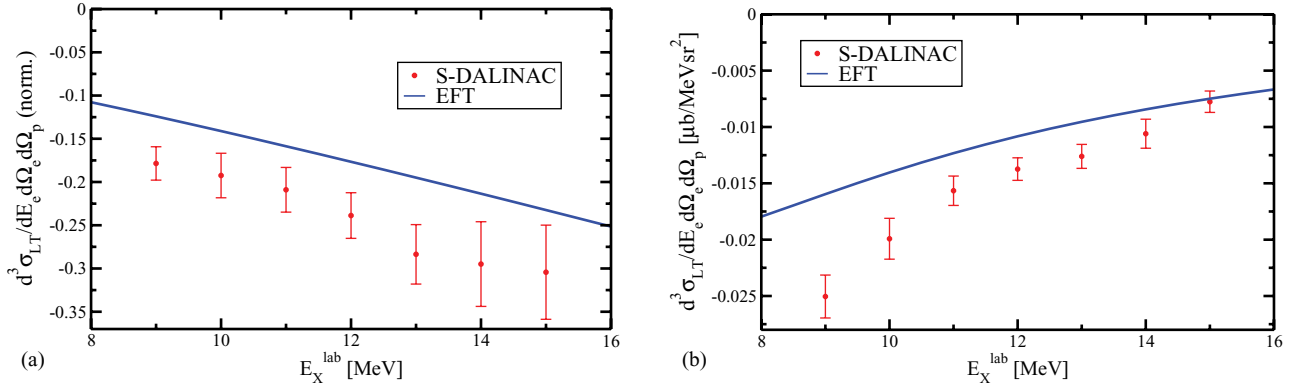
FIG. 10. (Color online) E_X^{lab} dependence of σ_{LT} at the minimum around $\Theta_p = 35°$, normalized (a) and absolute values (b), both for $E_0^{\text{lab}} = 85$ MeV, $\Theta_e^{\text{lab}} = 40°$.

bars, but the discrepancy at smaller energies and momentum transfers worsens (see Fig. 11).

E. Discussion of higher order contributions

In view of these discrepancies, one must investigate to what extent additional interactions could remedy the problem. The EFT($\not{\pi}$) result is complete up to N^{2}LO in electric and up to NLO in magnetic transitions, resulting in a conservative accuracy estimate of $\lesssim$10%, as discussed in Sec. III C. Including some renormalization-group-invariant subset of higher order contributions provides a third alternative to estimate the uncertainties of the calculation, besides order-by-order convergence and *prima facie* power counting.

However, the results so far provide a strong argument that higher order corrections cannot solve the problem: Recall first that σ_{LT} is nonzero only because of nonzero transverse components of the momentum $\vec{p}$ of the outgoing proton. If, in spite of the power counting, some higher order contributions were important for σ_{LT}, they should therefore contribute *more* at higher energies, where $\vec{p}$ is bigger and thus closer to the breakdown scale $\Lambda_{\not{\pi}}$. This would lead to larger higher order

corrections with increasing photon energy. This is however at odds with our analysis of Figs. 7 to 10. As fine-tuning could circumvent this general argument, we explicitly consider in the following some N^{3}LO contributions.

Magnetic transitions are negligible at these energies and in these kinematics, as seen in Figs. 5 and 6. Another contribution to electric transitions includes P-wave nucleon-nucleon final-state interactions, which also enter at N^{3}LO [33]. Although they do become stronger with increasing energy and momentum transfer, they are, even at high energies, not even of the same order of magnitude as the N^{2}LO contributions.

Next, one might think that the correction to the deuteron quadrupole moment of about 50% provided by the C_Q term in Eq. (2.16) can solve the problem at N^{3}LO. However, this term is at best comparable in size to the N^{2}LO term from SD mixing. Its contribution will thus be even smaller than the N^{2}LO correction in Figs. 7 and 8. An explicit calculation [34] renders

$$J_{ij}^0 = -2y_t D_t \frac{C_Q}{M\rho_d}\Big(q_i q_j - \frac{1}{3}\mathbf{q}^2 \delta_{ij}\Big), \quad \vec{J}_{ij} = 0. \quad (3.1)$$

The difference to the N^{2}LO result is less than 0.5% even at the minimum around $\Theta_p = 70°$ at $E_0^{\text{lab}} = 50$ MeV, $E_X^{\text{lab}} =$
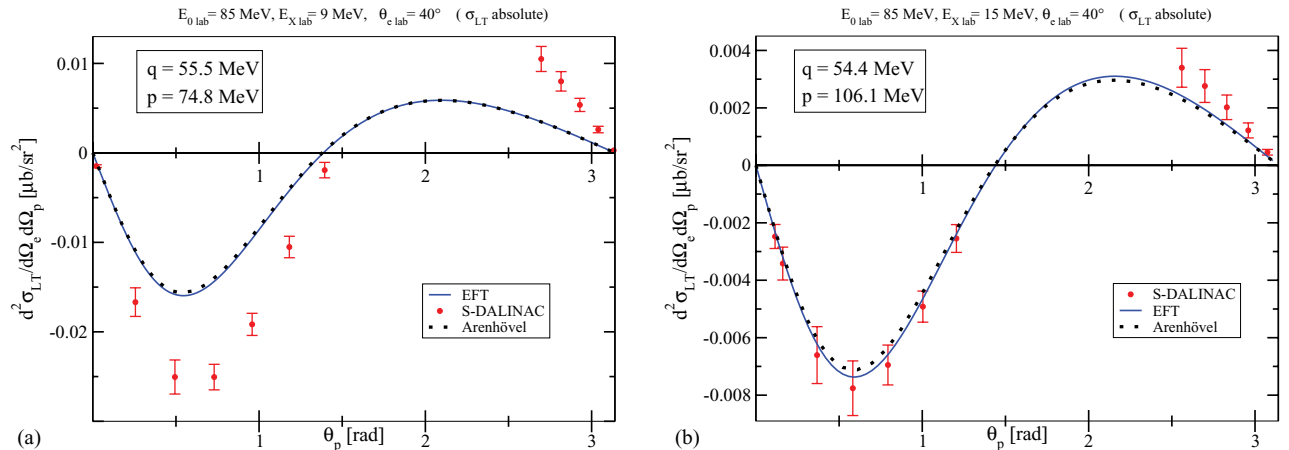
FIG. 11. (Color online) E_X^{lab} dependence of the *absolute* values of σ_{LT} for the extreme cases $E_X^{\text{lab}} = 9$ MeV (a) and 15 MeV (b) at $E_0^{\text{lab}} = 85$ MeV, $\Theta_e^{\text{lab}} = 40°$. Compare to the normalized data in Figs. 7 and 8.

$E_0^{lab} = 129$ MeV, $E_X^{lab} = 18$ MeV, $\theta_e^{lab} = 30°$
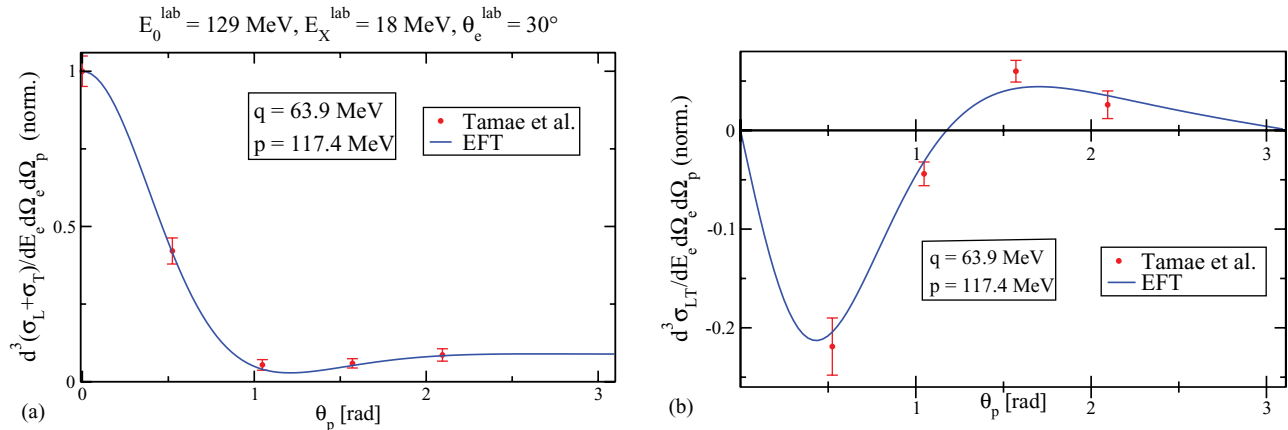
FIG. 12. (Color online) Comparison to the data of Ref. [8] for σ_{L+T} (a) and σ_{LT} (b), both in the laboratory frame (also for the hadronic variables!) and normalized to σ_{L+T} at $\Theta_p = 0$.

9 MeV, where the effect would need to be biggest to remedy the discrepancy. The contribution of this interaction to the interference terms σ_{LT} and σ_{TT} is furthermore zero since Eq. (3.1) is independent of Φ_p.

Corrections from relativistic kinematics are negligible. An example for a relativistic effect that is dynamical but has been neglected in our calculation is the spin-orbit interaction first considered in EFT($\not{\pi}$) by Chen *et al.* [43,44],

$$\mathcal{L}_{so} = iN^\dagger \left[\left(2\kappa_0 - \frac{1}{2} \right) + \left(2\kappa_1 - \frac{1}{2} \right) \tau_3 \right]$$
$$\times \frac{e}{8M^2} \vec{\sigma} \cdot (\vec{D} \times \vec{E} - \vec{E} \times \vec{D})N, \qquad (3.2)$$

where $\vec{E}$ is the electric field. This term is suppressed by $p_{typ}/M \lesssim Q^2$ relative to the magnetic field term in $\mathcal{L}_N$ [Eq. (2.14)] and thus enters in $M1_V$ transitions at N⁴LO. Chen *et al.* also demonstrated that it provides substantial angle-dependent contributions to deuteron Compton scattering at energies around $\omega \approx 49$ MeV [44]. Its Feynman diagrams are those of the LO magnetic transitions [Fig. 4.(m1-3)], with the magnetic moment interaction substituted by Eq. (3.2). The vector component of the hadronic current has the same structure as Eq. (2.27), and the zero-component can be written as

$$J_{hadr}^{0(M1_V)} = e\sqrt{Z}\epsilon^{ijk}\epsilon_{(d)}^i \frac{1}{\sqrt{8}} \left(N_p^\dagger \sigma_2 N_n^* \right) J_{jk}^0. \qquad (3.3)$$

The analytical results for these currents are reported in Ref. [34]. As expected, they give only a small correction to the already negligible NLO result for magnetic transitions. In σ_{L+T}, they lead to a correction never exceeding 10^{-3} of the LO result. Although they are Φ_p dependent, the relative difference to LO in σ_{LT} is less than 10^{-2}, with 2×10^{-3} at the extrema. In σ_{TT}, the relative difference to LO at the maximum is 10^{-5} and never exceeds 10^{-4}.

We mention in passing also a N⁴LO contribution that can naively be incorporated by modifying the dibaryon propagators [Eqs. (A12) and (A25)] to include the shape parameters $\rho_1 = 0.389$ fm³ for the ³S₁ channel and $r_1 = -0.48$ fm³ for

the ¹S₀ channel of NN scattering. This neglects diagrams that come from gauging the derivative terms in the Lagrangean that correspond to these corrections, so the result is not complete. However, we see that this leads only to minimal modifications of the structure functions. σ_{L+T} is increased by $\lesssim 5\%$ at back angles, by about 20% in the minimum due to fine-tuning, and in general by much less. σ_{LT} changes by less than 1% at the extrema, and σ_{TT} only by 0.1%.

Overall, this discussion supports our estimate of the theoretical uncertainty of our results.

F. A higher energy experiment

In Fig. 12, we finally compare the EFT($\not{\pi}$) results to an earlier experiment at a slightly higher momentum transfer [8], which reported good accord between data and the potential-model calculation by Arenhövel and co-workers[1] also for the normalized σ_{LT}. Although the involved proton momentum $p = 117$ MeV is even closer to the breakdown scale of EFT($\not{\pi}$) than for the S-DALINAC kinematics, we observe very good agreement for both σ_{L+T} and σ_{LT}. It is remarkable that the result describes the data so well in a regime in which EFT($\not{\pi}$) may start to become unreliable but deviates significantly from data at lower momenta.

IV. CONCLUDING QUESTIONS

In a parameter-free N²LO calculation using EFT($\not{\pi}$), a manifestly gauge and renormalization-group-invariant, well-tested formulation of few-nucleon physics with analytical results rooted in a systematic, model-independent low-energy expansion of all nuclear forces, with an *a priori* estimate of theoretical uncertainties corroborated by order-by-order

---

[1] For this experiment, the calculations were performed by using the Paris potential; its difference to the Bonn potential calculation in Refs. [4,5,7] should not be relevant here.

convergence, the S-DALINAC data on deuteron electrodisintegration $d(e, e'p)n$ at low energy and momentum transfer [5,6] cannot be explained.

Since an important aspect of any effective field theory is its universality and resulting model independence, this leads us to a conclusion beyond the EFT($\not{\pi}$) approach: The predictions of models that reproduce or share the input of EFT($\not{\pi}$) must agree with its results to within the accuracy of the EFT calculation, in the range where EFT($\not{\pi}$) is applicable. The analysis in Sec. III showed that the S-DALINAC data at low momentum and energy transfer lie undoubtedly within this regime. Therefore, any self-consistent potential model, irrespective of the detailed treatment of meson-exchange currents, "off-shell effects," cutoff dependence, etc. will to the accuracy outlined here agree with the EFT($\not{\pi}$) result, if it incorporates the same ingredients: the same deuteron binding energy, the same asymptotic normalization Z and asymptotic S-to-D wave ratio η_{sd} of the deuteron wave function, the same scattering length and effective range in the $^1S_0$ channel, the same isovectorial magnetic moment of the nucleon κ_1, and the same total radiative thermal capture cross section of neutrons on protons. This is nicely confirmed for electrodisintegration at low energies: The potential-model approach by Arenhövel and co-workers [4,5,7] yields essentially the same results as EFT($\not{\pi}$), especially for σ_{LT}.

We find furthermore that $\sigma_{L+T}, \sigma_{LT}$, and σ_{TT} are all dominated up to the few-percent level by the leading-order electric transition (i.e., by minimally coupling the photon to the nucleon and deuteron). This coupling is sensitive only to the asymptotics of the deuteron wave function. The statement is strongest for σ_{LT}, which shows the discrepancy: It is dominated up to the 1% level by only one LO electric process [Fig. 2.(e1)], that is, by the asymptotic normalization Z of the deuteron wave function [Eq. (2.19)]. In contradistinction, the discrepancy to the S-DALINAC data amounts to up to three standard deviations or 30%.

These findings suggest a re-analysis of the experiment [45]. We identified some questions concerning the kinematics and systematics of the experimental analysis and caution that the differences could in part arise from a dis-advantageous normalization of the data. If the discrepancies were confirmed, this would pose a highly nontrivial problem for nuclear theory. Only new data for deuteron electrodisintegration near threshold and at low momentum transfers can settle the issue definitively, particularly concerning the decomposition into the contributions of different structure functions. We are however confident to maintain that the validity and error estimate of the $E1_V$ part of the photodissociation cross section relevant for Big Bang nucleosynthesis as calculated in EFT($\not{\pi}$) [14,15,32,33] are not in question.

APPENDIX: CURRENTS AND INTEGRALS

We now list the analytical results for the hadronic currents described in Secs. II C and II D.

A. Useful loop integrals

The following loop integrals are calculated by the methodology outlined in Refs. [46,47],[2] using contour integration for the energy part and the PDS subtraction scheme combined with dimensional integration in D spatial dimensions [37,38] to identify divergences, parametrized by μ, and tensorial reduction. The reader may consult Ref. ([34] Appendix D) for details.

The fundamental bubble-sum integral is [37,38]

$$I_0^{(1)}(a) = \left(\frac{\mu}{2}\right)^{3-D} \int \frac{\mathrm{d}^D l}{(2\pi)^D} \frac{1}{(\vec{l} + \frac{\vec{q}}{2})^2 + a}$$

$$\stackrel{\mathrm{PDS}}{=} \frac{1}{4\pi}(\mu - \sqrt{a}). \tag{A1}$$

Reference [46] provides

$$I_0^{(2)}(a, b; q) = \int \frac{\mathrm{d}^3 l}{(2\pi)^3} \frac{1}{l^2 + a} \frac{1}{(\vec{l} + \frac{\vec{q}}{2})^2 + b}$$

$$= \frac{1}{2\pi q} \arctan\left(\frac{q}{2(\sqrt{a} + \sqrt{b})}\right). \tag{A2}$$

From that, one finds the μ-independent result with one loop momentum in the numerator,

$$A_1(a, b; q) = \int \frac{\mathrm{d}^D}{(2\pi)^D} \frac{\vec{l} \cdot \vec{q}}{l^2 + a} \frac{1}{(\vec{l} + \frac{\vec{q}}{2})^2 + b}$$

$$= I_0^{(1)}(a) - I_0^{(1)}(b) - \left(\frac{q^2}{4} + b - a\right) I_0^{(2)}(a, b; q), \tag{A3}$$

---

[2]We use a slightly different notation.

and the following μ-dependent ones with two powers of loop momenta in the numerator:

$$A_2(a, b; q) = \frac{1}{D-1} \int \frac{\mathrm{d}^D l}{(2\pi)^D} \frac{l^2 - \frac{(\vec{l}\cdot\vec{q})^2}{q^2}}{l^2 + a} \frac{1}{(\vec{l}+\frac{\vec{q}}{2})^2 + b}$$

$$= \frac{1}{1-D} \frac{1}{q^2} \left[\frac{2-D}{2} I_0^{(1)}(b) - a I_0^{(2)}(a, b; q) \right.$$

$$\left. + D \frac{\frac{q^2}{4} + b - a}{q^2} A_1(a, b; q) \right], \quad (A4)$$

$$B_2(a, b; q) = \frac{1}{1-D} \frac{1}{q^2} \int \frac{\mathrm{d}^D l}{(2\pi)^D} \frac{l^2 - D \frac{(\vec{l}\cdot\vec{q})^2}{l^2}}{l^2 + a} \frac{1}{(\vec{l}+\frac{\vec{q}}{2})^2 + b}$$

$$= \frac{1}{1-D} \frac{1}{q^2} \left[\frac{2-D}{2} I_0^{(1)}(b) - a I_0^{(2)}(a, b; q) \right.$$

$$\left. + D \frac{\frac{q^2}{4} + b - a}{q^2} A_1(a, b; q) \right]. \quad (A5)$$

Three powers of loop momenta in the numerator are covered by the integrals

$$A_3(a, b; q) = \frac{1}{(D-1)q^2} \int \frac{\mathrm{d}^D l}{(2\pi)^D} \frac{1}{l^2 + a} \frac{1}{(\vec{l}+\frac{\vec{q}}{2})^2 + b}$$

$$\times \left[(\vec{q}\cdot\vec{l}) l^2 - \frac{1}{q^2} (\vec{q}\cdot\vec{l})^3 \right]$$

$$= \frac{1}{(D-1)q^2} \left[-\frac{q^2}{2} I_0^{(1)}(b) - a A_1(a, b; q) \right.$$

$$\left. - \frac{1}{q^2} \hat{A}_3(a, b; q) \right], \quad (A6)$$

$$B_3(a, b; q) = \frac{D+2}{D-1} \frac{1}{q^6} \int \frac{\mathrm{d}^D l}{(2\pi)^D} \frac{1}{l^2 + a} \frac{1}{(\vec{l}+\frac{\vec{q}}{2})^2 + b}$$

$$\times \left[(\vec{q}\cdot\vec{l})^3 - \frac{3q^2}{D+2} (\vec{q}\cdot\vec{l}) l^2 \right]$$

$$= \frac{D+2}{D-1} \frac{1}{q^6} \left[\hat{A}_3(a, b; q) - \frac{3q^2}{D+2} \right.$$

$$\left. \times \left(-\frac{q^2}{2} I_0^{(1)}(b) - a A_1(a, b; q) \right) \right], \quad (A7)$$

with the aid of

$$\hat{A}_3(a, b; q)$$

$$= \int \frac{\mathrm{d}^D l}{(2\pi)^D} \frac{(\vec{q}\cdot\vec{l})^3}{l^2 + a} \frac{1}{(\vec{l}+\frac{\vec{q}}{2})^2 + b}$$

$$= -\frac{aq^2}{D} I_0^{(1)}(a) - \left(\frac{q^4}{4} - \frac{bq^2}{D} \right) I_0^{(1)}(b) + \left(\frac{q^2}{4} + b - a \right)$$

$$\times \left[-\frac{q^2}{2} I_0^{(1)}(b) + \left(\frac{q^2}{4} + b - a \right) A_1(a, b; q) \right]. \quad (A8)$$

B. Electric currents up to N²LO

The electric contributions to the hadronic current at LO are labeled as in Fig. 2. The four-vector contribution is for the first diagram with $\vec{r} := 2\vec{p} - \vec{q}$

$$J_{ij}^{0\,(\mathrm{e1})} = -2y_t D_p(\vec{p}; \omega, \vec{q}) \delta_{ij}; \quad \vec{J}_{ij}^{(\mathrm{e1})} = J_{ij}^{0\,(\mathrm{e1})} \frac{\vec{r}}{2M}, \quad (A9)$$

where the proton propagator

$$\mathrm{i}D_p(\vec{p}; \omega, \vec{q}) = \frac{\mathrm{i}}{-\omega + \frac{\vec{p}\cdot\vec{q}}{M} - \frac{q^2}{2M}} \quad (A10)$$

could be approximated for real photons by dropping the q^2 term in the denominator ($\omega = q$), but not in electrodisintegration because the kinematics imposes $\omega \sim q^2/M$.

The second diagram gives

$$J_{ij}^{0\,(\mathrm{e2})} = 2y_t D_t(p) \delta_{ij}; \quad \vec{J}_{ij}^{(\mathrm{e2})} = -J_{ij}^{0\,(\mathrm{e2})} \frac{\vec{q}}{4M}, \quad (A11)$$

with the spin-triplet dibaryon propagator

$$\mathrm{i}D_t(p) = \frac{M\rho_d}{2} \frac{\mathrm{i}}{\gamma - \frac{\rho_d}{2}(\gamma^2 + p^2) + \mathrm{i}p}. \quad (A12)$$

After integrating over the loop, diagram (3) results in

$$J_{ij}^{0\,(\mathrm{e3})} = -2y_t^3 D_t(p) M^2 I_0^{(2)}(-p^2, \gamma^2) \delta_{ij}, \quad (A13)$$

$$\vec{J}_{ij}^{(\mathrm{e3})} = y_t^3 D_t(p) M \left[I_0^{(2)}(-p^2, \gamma^2) + \frac{2}{q^2} A_1(-p^2, \gamma^2; q) \right]$$

$$\times \vec{q}\, \delta_{ij}. \quad (A14)$$

Here, as in the following, $-p^2$ is understood to be $-p^2 - \mathrm{i}\epsilon$ with $\epsilon \searrow 0$ (i.e., $\sqrt{-p^2} = -\mathrm{i}p$, where p is the proton momentum).

The N²LO contributions come from SD-mixing operators only. Following the numeration of Fig. 3, one finds

$$J_{ij}^{0\,(\mathrm{sd1})} = -\frac{1}{2} \frac{C_{sd}}{\sqrt{M\rho_d}} D_p(\vec{p}; \omega, \vec{q}) \left(r_i r_j - \frac{1}{3} \vec{r}^2 \delta_{ij} \right),$$

$$\vec{J}_{ij}^{(\mathrm{sd1})} = J_{ij}^{0\,(\mathrm{sd1})} \frac{\vec{r}}{2M}, \quad (A15)$$

$$J_{ij}^{0\,(\mathrm{sd2})} = \frac{C_{sd}}{\sqrt{M\rho_d}} D_t(p) \left(p_i p_j - \frac{1}{3} \vec{p}^2 \delta_{ij} \right),$$

$$\vec{J}_{ij}^{(\mathrm{sd2})} = -J_{ij}^{0\,(\mathrm{sd2})} \frac{\vec{q}}{4M}, \quad (A16)$$

$$J_{ij}^{0\,(\mathrm{sd3})} = -2 \frac{C_{sd} y_t^2}{\sqrt{M\rho_d}} D_t(p) M^2 I_0^{(2)}(-p^2, \gamma^2; q)$$

$$\times \left(p_i p_j - \frac{1}{3} \vec{p}^2 \delta_{ij} \right), \quad (A17)$$

$$\vec{J}_{ij}^{(\mathrm{sd3})} = \frac{C_{sd} y_t^2}{\sqrt{M\rho_d}} D_t(p) M \left[I_0^{(2)}(-p^2, \gamma^2; q) \right.$$

$$\left. + \frac{2}{q^2} A_1(-p^2, \gamma^2; q) \right] \left(p_i p_j - \frac{1}{3} \vec{p}^2 \delta_{ij} \right) \vec{q}, \quad (A18)$$

$$J_{ij}^{0\,(\mathrm{sd4+sd5})} = -2 \frac{C_{sd} y_t^2}{\sqrt{M\rho_d}} D_t(p) M^2 [B_2(-p^2, \gamma^2; q)$$

$$+ B_2(\gamma^2, -p^2; q)] \left(q_i q_j - \frac{1}{3} \vec{q}^2 \delta_{ij} \right), \quad (A19)$$

$$\left(\vec{J}_{ij}^{(\text{sd4+sd5})}\right)_k = 2\frac{C_{sd}}{\sqrt{M\rho_d}}D_t(p)y_t^2 M\left[\frac{1}{2}B_2(-p^2,\gamma^2;q)\right.$$

$$\times\left(q_iq_j - \frac{1}{3}\vec{q}^2\delta_{ij}\right)q_k + [A_3(-p^2,\gamma^2;q)$$

$$- A_3(\gamma^2,-p^2;q)]\left(q_i\delta_{jk} + q_j\delta_{ik} - \frac{2}{3}q_k\delta_{ij}\right)$$

$$+ [B_3(-p^2,\gamma^2;q) - B_3(\gamma^2,-p^2;q)]$$

$$\left.\times\left(q_iq_jq_k - \frac{1}{3}q^2q_k\delta_{ij}\right)\right]. \tag{A20}$$

The last three diagrams contribute only to the three-vector component of the current:

$$\left(\vec{J}_{ij}^{(\text{sd6})}\right)_k = \frac{C_{sd}}{\sqrt{M\rho_d}}\left[-p_i\delta_{jk} + \left(-p_j + \frac{1}{2}q_j\right)\delta_{ik}\right.$$

$$\left.+ \frac{2}{3}\left(p_k - \frac{1}{4}q_k\right)\delta_{ij}\right], \tag{A21}$$

$$\left(\vec{J}_{ij}^{(\text{sd7+sd8})}\right)_k = \frac{C_{sd}}{\sqrt{M\rho_d}}D_t(p)y_t^2\frac{M}{4}\left[I_0^{(1)}(\gamma^2) - I_0^{(1)}(-p^2)\right]$$

$$\times\left(q_j\delta_{ik} + q_i\delta_{jk} - \frac{2}{3}q_k\delta_{ij}\right). \tag{A22}$$

With these results, it is simple to show that the LO and N^{2}LO electric currents are separately gauge invariant ($q_\mu J_{ij}^\mu = 0$). It is also noteworthy that the total current at each order is independent of the regularization parameter μ.

C. Magnetic currents up to NLO

The LO diagrams, numbered as in Fig. 4, contribute

$$\vec{J}^{(\text{m1})} = -y_t D_p(\vec{p};\omega,\vec{q})\frac{\kappa_1}{M}\vec{q}, \vec{J}^{(\text{m2})}$$

$$= -y_t D_n(\vec{p};\omega,\vec{q})\frac{\kappa_1}{M}\vec{q}, \tag{A23}$$

$$\vec{J}^{(\text{m3})} = -2y_t D_s(p)y_s^2\kappa_1 M I_0^{(2)}(-p^2,\gamma^2;q)\vec{q}, \tag{A24}$$

with neutron propagator $D_n(\vec{p};\omega,\vec{q}) = D_p(-\vec{p};\omega,\vec{q})$ and spin-singlet dibaryon propagator

$$iD_s(p) = \frac{Mr_0}{2}\frac{i}{\frac{1}{a_0} - \frac{r_0}{2}p^2 + ip}. \tag{A25}$$

The current provided by the NLO contribution is

$$\vec{J}^{(\text{m4})} = -2y_s D_s(p)\frac{L_1}{M\sqrt{r_0\rho_d}}\vec{q}. \tag{A26}$$

Notice that these currents are all transversal only.

[1] H. Arenhövel and M. Sanzone, *Photodisintegration of the Deuteron* (Springer-Verlag, Berlin, 1991).
[2] R. A. Gilman and F. Gross, J. Phys. G **28**, R37 (2002).
[3] W. Fabian and H. Arenhövel, Nucl. Phys. **A314**, 253 (1979).
[4] H. Arenhövel, W. Leidemann, and E. L. Tomusiak, Eur. Phys. J. A **23**, 147 (2005).
[5] P. von Neumann-Cosel *et al.*, Phys. Rev. Lett. **88**, 202304 (2002).
[6] Reported at the Web site of the experiment, http://qclam.ikp.physik.tu-darmstadt.de/eng/exp_deep.htm.
[7] H. Arenhövel (private communication).
[8] T. Tamae *et al.*, Phys. Rev. Lett. **59**, 2919 (1987).
[9] K. M. Nollett and S. Burles, Phys. Rev. D **61**, 123505 (2000).
[10] R. H. Cyburt, Phys. Rev. D **70**, 023505 (2004).
[11] N. Ryezayeva *et al.*, Phys. Rev. Lett. (to appear).
[12] W. Tornow *et al.*, Phys. Lett. **B574**, 8 (2003).
[13] H. Weller (private communication).
[14] G. Rupak, Nucl. Phys. **A678**, 405 (2000).
[15] S. Ando, R. H. Cyburt, S. W. Hong, and C. H. Hyun, Phys. Rev. C **74**, 025809 (2006).
[16] L. E. Marcucci, K. M. Nollett, R. Schiavilla, and R. B. Wiringa, Nucl. Phys. **A777**, 111 (2006).
[17] P. F. Bedaque and U. van Kolck, Phys. Lett. **B428**, 221 (1998).
[18] P. F. Bedaque, H.-W. Hammer, and U. van Kolck, Phys. Rev. C **58**, R641 (1998).
[19] P. F. Bedaque and H. W. Grießhammer, Nucl. Phys. **A671**, 357 (2000).
[20] F. Gabbiani, P. F. Bedaque, and H. W. Grießhammer, Nucl. Phys. **A675**, 601 (2000).
[21] G. Rupak and X. W. Kong, Nucl. Phys. **A717**, 73 (2003).
[22] S. R. Beane and M. J. Savage, Nucl. Phys. **A694**, 511 (2001).
[23] S. I. Ando and C. H. Hyun, Phys. Rev. C **72**, 014008 (2005).
[24] U. van Kolck, Prog. Part. Nucl. Phys. **43**, 337 (1999).
[25] S. R. Beane, P. F. Bedaque, W. C. Haxton, D. R. Phillips, and M. J. Savage, in *At the Frontier of Particle Physics*, edited by M. Shifman (World Scientific, Singapore, 2001), Vol. 1, p. 133.
[26] D. R. Phillips, Czech. J. Phys. **52**, B49 (2002).
[27] P. F. Bedaque and U. van Kolck, Annu. Rev. Nucl. Part. Sci. **52**, 339 (2002).
[28] L. Platter, H. W. Hammer, and Ulf-G. Meissner, Phys. Rev. A **70**, 052101 (2004).
[29] L. Platter, H. W. Hammer, and U. G. Meissner, Phys. Lett. **B607**, 254 (2005).
[30] H. W. Hammer and L. Platter, Eur. Phys. J. A **32**, 113 (2007).
[31] I. Stetcu, B. R. Barrett, and U. van Kolck, Phys. Lett. **B653**, 358 (2007).
[32] J. W. Chen, G. Rupak, and M. J. Savage, Phys. Lett. **B464**, 1 (1999).
[33] J. W. Chen and M. J. Savage, Phys. Rev. C **60**, 065205 (1999).
[34] S. Christlmeier, Diplom thesis, Technische Universität München, 2004, available (in English) at http://www.physik.tu-muenchen.de/lehrstuehle/T39/T39_files/T39_people_files/DipThesis/christlmeier.pdf.
[35] H. Arenhövel, W. Leidemann, and E. L. Tomusiak, Phys. Rev. C **46**, 455 (1992).
[36] D. B. Kaplan, Nucl. Phys. **B494**, 471 (1997).
[37] D. B. Kaplan, M. J. Savage, and M. B. Wise, Phys. Lett. **B424**, 390 (1998).
[38] D. B. Kaplan, M. J. Savage, and M. B. Wise, Nucl. Phys. **B534**, 329 (1998).
[39] D. R. Phillips, G. Rupak, and M. J. Savage, Phys. Lett. **B473**, 209 (2000).

[40] A. E. Cox, S. A. R. Wynchank, and C. H. Collie, Nucl. Phys. **74**, 497 (1965).

[41] H. W. Grießhammer and G. Rupak, Phys. Lett. **B529**, 57 (2002).

[42] H. W. Grießhammer, Nucl. Phys. **A744**, 192 (2004).

[43] J. W. Chen, X. D. Ji, and Y. C. Li, Phys. Lett. **B603**, 5 (2004).

[44] J. W. Chen, X. D. Ji, and Y. C. Li, Phys. Lett. **B620**, 33 (2005).

[45] A. Shevchenko and P. von Neumann-Cosel (private communication).

[46] M. J. Savage and R. P. Springer, Nucl. Phys. **A686**, 413 (2001).

[47] S. Fleming, T. Mehen, and I. W. Stewart, Nucl. Phys. **A677**, 313 (2000).